Fourier Optics: Derivation and Applications

Final Report on Fundamentals of Electro-optics

Teammates：電機一 B10901042 彭瑄、電機一 B10901065 林奕樺

2022.06.03

$$\mathcal{F}\{A(x,y)\}\left(\frac{x'}{L\lambda},\frac{y'}{L\lambda}\right)=\left[\iint_{\mathbb{R}^2}A(x,y)e^{-i2\pi(\nu_x x+\nu_y y)}\mathrm{d}x\mathrm{d}y\right]_{\substack{\nu_x=\frac{x'}{L\lambda}\\ \nu_y=\frac{y'}{L\lambda}}}$$

"It is evident that it [Fourier series] includes an entire series of distinct phenomena, and that the study of it cannot be omitted without losing a notable part of the science of nature."

--Joseph Fourier

Abstract

The following passage focuses on three parts: the derivation of the Fourier optics equation, Fourier transform in polar coordinates, and lastly, applications of Fourier optics.

We shall derive the equation for Fourier optics in two settings: diffraction through an aperture, and imaging through a focusing lens.

Next, we shall provide detailed derivation of the Fourier transform for radially dependent functions, noting its relationship with the Hankel transform, leading up to the Fourier transform of the cylinder function, and obtain the sombrero function.

Lastly, we provided three theoretical applications of Fourier optics, which are DNA X-ray crystallography, mechanism of zone plates, and reciprocal lattices respectively.

Table of Contents

0. Teammate

EE1 B10901042 彭瑎

EE1 B10901065 林奕樺

- Contributions:

  彭　瑎:

  Derivation on Fourier Optics-Through a Focusing Lens

  Hankel Transform

  Application of Fourier Optics on Theoretical Settings-DNA X-ray Crystallography

  Application of Fourier Optics on Theoretical Settings-Reciprocal Lattice

  林奕樺:

  Derivation on Fourier Optics-Through an Aperture

  Application of Fourier Optics on Theoretical Settings-DNA X-ray Crystallography

  Application of Fourier Optics on Theoretical Settings-Zone Plates

1. Derivation on Fourier Optics

1.1. Through an Aperture

1.1.1. 1D Condition, Through a Slit

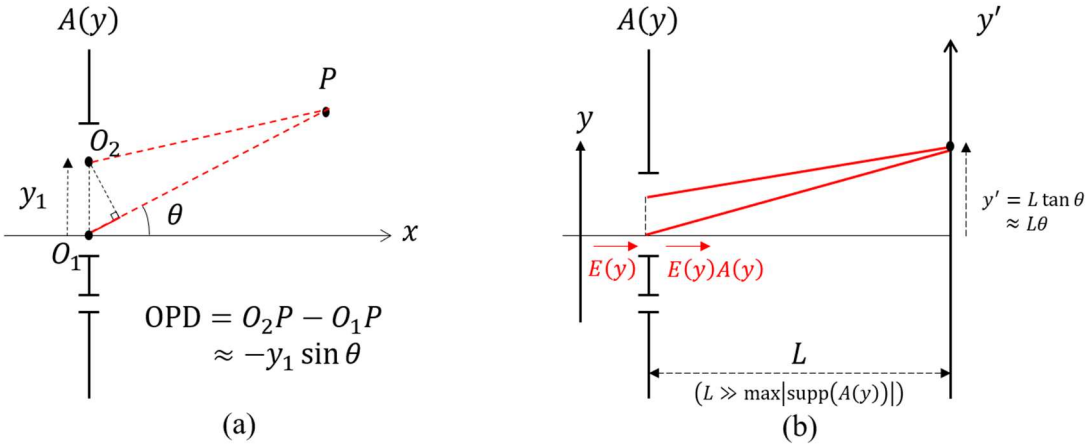

Figure 1.1 (ray through a slit)

First, we take a 1D single slit (it is not necessary to be a single slit) as an example. As shown in figure 1.1-(a), we only consider the angle θ between O_1P and the x-axis, and the optical path difference (OPD) between O_1P and O_2P. In figure 1.1-(a) we can see that

$$\text{OPD} = O_2P - O_1P \approx -y_1 \sin\theta \tag{1-1}$$

And the phase difference δ between O_1P and O_2P is

$$\delta = \frac{2\pi}{\lambda} \cdot \text{OPD} = -y_1 \frac{2\pi \sin\theta}{\lambda} \tag{1-2}$$

In figure 1.1-(b), we place an observation plane at $x = L$. Let $A(y)$ be the function describing the slit/aperture, called the *aperture function*. Because L is far greater than the size of the aperture[1], we can apply the paraxial approximation of $\sin\theta \approx \theta \approx y'/L$. Thus, the phase difference becomes

$$\delta = -2\pi y_1 \frac{y'}{L\lambda} = -2\pi\nu y_1, \qquad \nu = \frac{y'}{L\lambda} \tag{1-3}$$

Let the amplitude of the incidence ray be $E(y)$ (its electric field), the light strength just exiting the aperture will be $E(y)A(y)$, and the total ray amplitude at (L, y') will thus be

$$\int_{-\infty}^{\infty} E(y)A(y)e^{i\delta}\mathrm{d}y = \int_{-\infty}^{\infty} E(y)A(y)e^{-i2\pi\nu y}\mathrm{d}y \coloneqq \mathcal{F}\{E(y)A(y)\}(\nu) \tag{1-4}$$

Notice that the formula above is the Fourier integral of $E(y)A(y)$, where $\mathcal{F}\{\cdot\}$ denotes the *Fourier transformation*!

[1] Rephrased using mathematical jargon: $L \gg \max|\text{supp}(A(y))|$, the greatest value of the *support* (y where $A(y) \neq 0$) of the aperture function.

Because the light intensity is $I \propto E^2$, and by setting the electric field strength as a constant, the light intensity distribution on the observation plane $x = L$ is

$$I\left(\frac{y'}{L\lambda}\right) \propto \left[\mathcal{F}\{A(y)\}\left(\frac{y'}{L\lambda}\right)\right]^2 \tag{1-5}$$

This result is called the "Fraunhofer approximation."

1.1.2. 2D Condition, Through an Aperture

We use the same method as we used in 1.1.1.

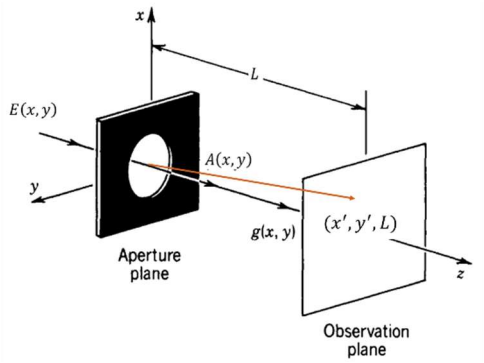

Figure 1.2 (ray through an aperture)

As the aperture system shown in figure 1.2, suppose there are two rays start from $(0,0,0)$ and $(x, y, 0)$ to (x', y', L). Let $r_1 = \sqrt{x'^2 + y'^2 + L^2}$ and $r_2 = \sqrt{(x'-x)^2 + (y'-y)^2 + L^2}$, under the *paraxial condition* ($L \gg \sqrt{x'^2 + y'^2}$, $x' \gg x$ and $y' \gg y$), the OPD between r_1 and r_2 is

$$r_1 \approx L + \frac{x'^2 + y'^2}{2L}, \quad r_2 \approx L + \frac{(x'-x)^2 + (y'-y)^2}{2L} \tag{1-6}$$

$$\text{OPD} = r_2 - r_1 \approx -\left(x\frac{x'}{L} + y\frac{y'}{L}\right) \tag{1-7}$$

Let $\nu_x = \frac{x'}{L\lambda}$, $\nu_y = \frac{y'}{L\lambda}$. The phase difference δ is

$$\delta = \frac{2\pi}{\lambda} \cdot \text{OPD} = -2\pi(x\nu_x + y\nu_y) \tag{1-7}$$

Let $A(x, y)$ be the aperture function and the amplitude of the incidence ray be $E(x, y)$, then the total amplitude at (x', y', L) will be

$$\begin{aligned} \iint_{\mathbb{R}} E(x,y)A(x,y)e^{i\delta}\,dxdy &= \iint_{\mathbb{R}} E(x,y)A(x,y)e^{-i2\pi(x\nu_x + y\nu_y)}\,dxdy \\ &:= \mathcal{F}\{E(x,y)A(x,y)\}(\nu_x, \nu_y) \end{aligned} \tag{1-8}$$

Therefore, the intensity distribution is

$$I\left(\frac{x}{L\lambda}, \frac{y}{L\lambda}\right) \propto \left[\mathcal{F}\{E(x,y)A(x,y)\}\left(\frac{x}{L\lambda}, \frac{y}{L\lambda}\right)\right]^2 \tag{1-9}$$

1.2. Through a Focusing Lens

Take a 1D lens for example, the following arguments can be easily extended to the 2D case. As shown in figure (1.3), we have a system with a picture on the frontal focal point of a focusing lens, and an imaging plane at the rear focal plane. An input ray with wavevector $\boldsymbol{k}$ coming from the left shines onto the picture of desire, then it will scatter into different directions.

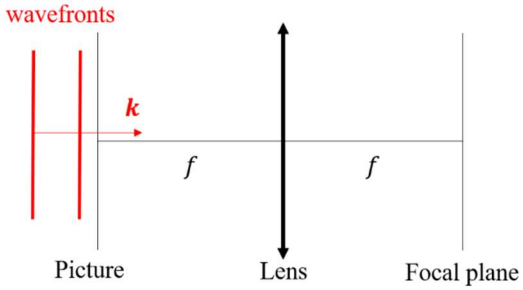

Figure 1.3 (2*f*-system setup)

Denote α as the scattering angle of a ray. From figure 1.4-(a), we can see that the ray leaves a pattern of spatial period L on the picture. One of the many rays that have an inclination angle of α will go through the *nodal point* of the lens, thus not changing its direction after the refraction. From figure 1.4-(b) we can see that all the parallel rays will focus on the point x' on the focal plane.

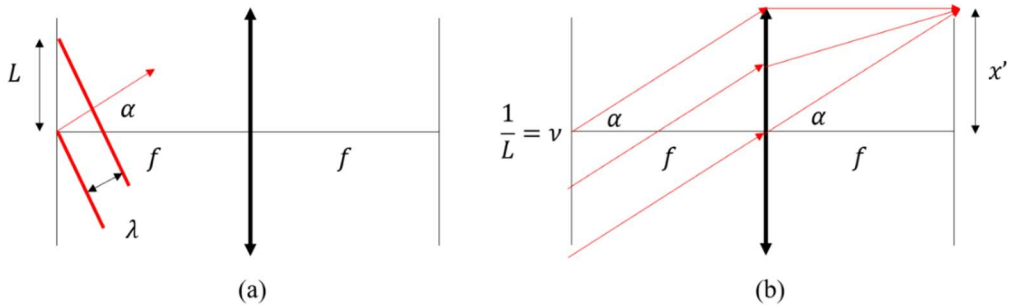

Figure 1.4 (rays through focusing lens)

We can also see from the figures above, using paraxial approximations, that

$$\begin{cases} x' \approx f\alpha \\ L\alpha \approx \lambda \end{cases} \rightarrow x' = \frac{f\lambda}{L} \coloneqq f\lambda\nu \tag{1-10}$$

Where ν is the spatial frequency associated with the spatial period of L. Amazingly, a *one-to-one correspondence* between the spatial frequency ν and the imaging location x' can be spotted, namely

$$\nu \leftrightarrow x'/f\lambda \tag{1-11}$$

And in order to obtain the total magnitude of electric field at x' we just need to find the magnitude of the frequency ν in the initial image, which is its Fourier transform! Thus, we obtain

$$E(x') = \int_{\mathbb{R}} A(x)e^{-i2\pi\nu}\ \mathrm{d}x\Big|_{\nu=x'/f\lambda} \tag{1-12}$$

2. Hankel Transform

2.1. What are Bessel Functions

Bessel functions are, to put it simply, solutions to the *Bessel differential equation*:

$$x^2\frac{\mathrm{d}y}{\mathrm{d}x}+x\frac{\mathrm{d}y}{\mathrm{d}x}+(x^2-\nu^2)y=0. \tag{2-1}$$

An infinite series solution can be obtained by the *Frobenius method*: setting

$$y=x^r\sum_{n=0}^{\infty}a_nx^n \qquad r\in\mathbb{R}$$

Substitute it back into equation (2-1), and we will obtain:

$$(n+r-\nu)(n+r+\nu)a_n+a_{n-2}=0$$

For $n=0\rightarrow r=\pm\nu=\nu$, and let $a_0=1, a_1=0$, we have:

$$a_n=\frac{-a_{n-2}}{n(n+2\nu)}=\begin{cases}0, & n=2m+1 \text{ is odd;}\\ \dfrac{(-1)^m\cdot 2^{-2m}}{m!\,(m+\nu)!}, & n=2m \text{ is even.}\end{cases}$$

$$\rightarrow J_\nu(x)=\sum_{n=0}^{\infty}\frac{(-1)^n}{n!\,(n+\nu)!}\left(\frac{x}{2}\right)^{2n+\nu} \tag{2-2}$$

This is known as the *Bessel function of the first kind of order* ν. Note that if ν is not an integer, the factorial function should be replaced by the gamma function.

2.2. Order Reduction of Bessel Functions

A useful property of the Bessel functions is:

$$\frac{\mathrm{d}}{\mathrm{d}x}[x^\nu J_\nu(x)]=x^\nu J_{\nu-1}(x) \tag{2-3}$$

, the derivation is as follow:

$$\frac{\mathrm{d}}{\mathrm{d}x}[x^\nu J_\nu(x)]=\frac{\mathrm{d}}{\mathrm{d}x}\left[\sum_{n=0}^{\infty}\frac{(-1)^n}{n!\,(n+\nu)!}\left(\frac{x}{2}\right)^{2n+2\nu}\right]$$

$$=\sum_{n=0}^{\infty}\frac{(-1)^n(n+\nu)}{n!\,(n+\nu)!}\left(\frac{x}{2}\right)^{2n+2\nu-1}=\sum_{n=0}^{\infty}\frac{(-1)^n}{n!\,(n+\nu-1)!}\left(\frac{x}{2}\right)^{2n+2\nu}$$

$$=x^\nu\sum_{n=0}^{\infty}\frac{(-1)^n}{n!\,(n+\nu-1)!}\left(\frac{x}{2}\right)^{2n+(\nu-1)}=x^\nu J_{\nu-1}(x)$$

Thus, it is proven.

2.3. Generating Function

The generating function for Bessel functions of integer orders is

$$e^{\frac{x}{2}\left(t-\frac{1}{t}\right)} = \sum_{n=-\infty}^{\infty} J_n(x)t^n \tag{2-4}$$

The proof of equation (2-4) is as follow.

$$e^{\frac{x}{2}\left(t-\frac{1}{t}\right)} = \sum_{m=0}^{\infty}\frac{1}{m!}\left(\frac{x}{2}t\right)^m \sum_{n=0}^{\infty}\frac{1}{n!}\left(\frac{x}{2}\ \frac{-1}{t}\right)^n = \sum_{n=0}^{\infty}\sum_{m=0}^{\infty}\frac{1}{m!}\left(\frac{x}{2}t\right)^m \frac{1}{n!}\left(\frac{x}{2}\ \frac{-1}{t}\right)^n$$

$$= \sum_{n=0}^{\infty}\sum_{k+n=0}^{\infty}\frac{(-1)^m}{(n+k)!\,n!}\left(\frac{x}{2}\right)^{2n+k} t^n = \sum_{n=0}^{\infty}\sum_{k=-\infty}^{\infty}\frac{(-1)^m}{(n+k)!\,n!}\left(\frac{x}{2}\right)^{2n+k} t^n$$

$$= \sum_{k=-\infty}^{\infty} J_k(x)\cdot t^k$$

The last equality comes directly from our series definition of Bessel functions in equation (2-2).

2.4. Integral Definition of Bessel Functions

The series definition of equation (2-2) is really useful in numerical analysis of the Bessel functions, but in order to dive deeper into their theoretical applications, we should derive an integral definition of it.

A theorem is needed for our derivation, the theorem will be stated without proof since it is outside the scope of this report.

Theorem:

Let $C: |z| = 1$ *be a counter-clockwise contour in the complex plane, then we have the following contour integral of*

$$\frac{1}{2\pi i}\oint_C z^m \mathrm{d}z = \begin{cases} 1, & m = -1; \\ 0, & m \neq -1. \end{cases} \tag{2-5}$$

The theorem above is just a simple case of the famous *Cauchy integral formula* in complex analysis, related to the residues of functions. Now, let us begin the derivation of the integral definition of Bessel functions.

Note that

$$\frac{1}{2\pi i}\oint_C \left(\sum_{n=-\infty}^{\infty} f_n t^n\right) t^m \mathrm{d}t = f_{-m-1}$$

$$\rightarrow J_n(x) = \frac{1}{2\pi i}\oint_C \left(\sum_{n=-\infty}^{\infty} f_n t^n\right) t^{-n-1}\mathrm{d}t = \frac{1}{2\pi i}\oint_C e^{\frac{x}{2}\left(t-\frac{1}{t}\right)} \cdot t^{-n-1}\,\mathrm{d}t$$

Using the substitution $t = e^{i\theta}$, $\mathrm{d}t = it\,\mathrm{d}\theta$

$$J_n(x) = \frac{1}{2\pi}\int_{2\pi} e^{\frac{x}{2}(e^{i\theta}-e^{-i\theta})} e^{-in}\,\mathrm{d}\theta = \frac{1}{2\pi}\int_{2\pi} e^{-i(n\theta - x\sin\theta)}\,\mathrm{d}\theta$$

Thus, we obtain the following integral definition of Bessel functions:

$$J_n(x) = \frac{1}{2\pi}\int_{2\pi} e^{-i(nt - x\sin t)}\,\mathrm{d}t \tag{2-6}$$

The bound of the integral is any interval with length 2π.

2.5. Hankel Transform

We already have the Fourier transform in cartesian coordinates, let us now represent it in the polar coordinate with the following change of variables:

$$\begin{cases} x = r\cos\theta \\ y = r\sin\theta \end{cases} \leftrightarrow \begin{cases} u = \rho\cos\phi \\ v = \rho\sin\phi \end{cases}$$

Consider a simple case where the function being transformed is only radially-dependent, i.e. $f = f(r)$. Then we have

$$\mathcal{F}\{f(r)\} = \iint_{\mathbb{R}} f(r) e^{-i2\pi(ux+vy)}\mathrm{d}x\,\mathrm{d}y$$

$$= \int_{2\pi}\int_0^{\infty} f(r) e^{-i2\pi\rho\,(\cos\phi\cos\theta + \sin\phi\sin\,)} r\,\mathrm{d}r\,\mathrm{d}\theta$$

$$= \int_0^{\infty} r\cdot f(r)\int_{2\pi} e^{-i2\pi\rho r\cos(\phi-\theta)}\,\mathrm{d}\theta\,\mathrm{d}r$$

$$= 2\pi\int_0^{\infty} f(r)\cdot r\,J_0(2\pi\rho r)\,\mathrm{d}r \tag{2-7}$$

The last integral (without the 2π constant) is known as the *Hankel transform of order 0*. Here we provided the Hankel transform of order n and its inverse transform.

$$\mathcal{H}_n\{f(r)\} = \int_0^{\infty} r\,f(r)\,J_n(2\pi\rho r)\,\mathrm{d}r = F_n(\rho) \tag{2-8}$$

$$\mathcal{H}_n^{-1}\{F_n(\rho)\} = \int_0^{\infty} \rho\,F_n(\rho)\,J_n(2\pi\rho r)\,\mathrm{d}\rho = f(r) \tag{2-9}$$

Hankel transform is equivalent to the Fourier transform by replacing the complex exponential functions with Bessel functions as the basis of decomposition! In fact, Hankel transforms are also known as the *Fourier-Bessel transformation*, their relationship is deeply connected with the *Sturm-Liouville equation* and the orthogonality of functions.

2.6. A Classic Example

With all the needed tools derived, let us now consider the Fourier transform of the classic *cylinder function*.

$$\mathrm{cyl}\left(\frac{\mathrm{r}}{\mathrm{D}}\right) = \begin{cases} 1, & |r| < \dfrac{D}{2} \\ 0, & |r| > \dfrac{D}{2} \end{cases}$$

$$\begin{aligned} \mathcal{F}\left\{\mathrm{cyl}\left(\frac{r}{D}\right)\right\}(\rho) &= 2\pi \cdot \mathcal{H}_0\left\{\mathrm{cyl}\left(\frac{r}{D}\right)\right\} \\ &= 2\pi \int_0^{\infty} \mathrm{cyl}\left(\frac{r}{D}\right) \cdot r\, J_0(2\pi\rho r)\, \mathrm{d}r = 2\pi \int_0^{D/2} r\, J_0(2\pi\rho r)\, \mathrm{d}r \\ &= \frac{2\pi}{(2\pi\rho)^2} \int_0^{\pi D\rho} (2\pi\rho r)\, J_0(2\pi\rho r)\, \mathrm{d}(2\pi\rho r) = \frac{1}{2\pi\rho^2}\left[t\, J_1(t)\right]_0^{\pi D\rho} \\ &= \frac{D}{2\rho} J_1(\pi D\rho) = D^2 \frac{\pi}{4}\left[\frac{2J_1(\pi D\rho)}{\pi D\rho}\right] = \frac{\pi}{4} D^2 \mathrm{somb}(D\rho) \end{aligned}$$

The equality sign in the third line utilizes equation (2-3), the order reduction formula of Bessel functions. And surprisingly, the result we obtained is the sombrero function, defined as

$$\mathrm{somb}(r) = \frac{2J_1(\pi r)}{\pi r} \tag{2-10}$$

3. Application of Fourier Optics on Theoretical Settings

3.1. DNA X-ray Crystallography

The structure of DNA (deoxyribonucleic acid) is a double helix, like two springs intertwined together. To study the structure of DNA, let us first examine the theoretical diffraction pattern of a single helix. Then, we will compare the theoretical expectations with actual experimental results conducted by ourselves. And lastly, we shall analyze the real DNA X-ray diffraction pattern photographed by the team led by Franklin Rosalind in 1953.

3.1.1. Theoretical Expectations of Single Helix Diffraction

Let us start simple with the single helix. As shown below in figure 3.1, a single helix has two different families of parallel lines, one going from top right to bottom left and another from top left down to bottom right, each representing the part of the helix that is closer or further away from the observer respectively. These two families of lines with equal spacing of Δ can be thought of as impulse trains, thus creating an interference pattern.

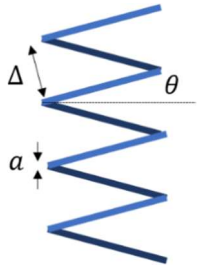

Figure 3.1 (single helix)

Aside from the spacing, suppose the thickness of the strand that makes up the helix is of width a, and the inclination of the family of parallel lines is θ. This is essentially a multi-slit interference experiment (if the helix size is finite), but with two directions of periodicity. The two families of parallel lines create an "X" shaped cross with a tilt of angle θ, and the interference pattern of multiple slits can be seen spanning across the "X".

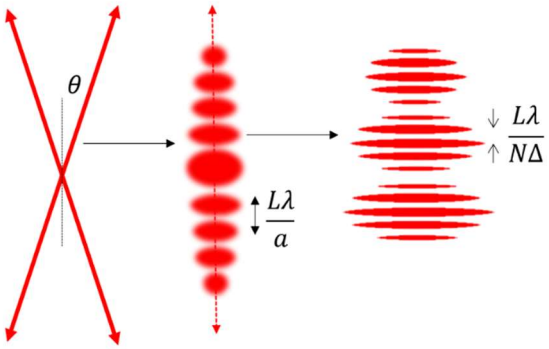

Figure 3.2 (theoretical expectation of single helix diffraction)

We know that the interference pattern of N equal slits of width a, each separated by a distance of Δ, is

$$\text{Intensity} \propto \underbrace{\left(\frac{\sin\frac{\pi a}{L\lambda}x}{\frac{\pi a}{L\lambda}x}\right)^2}_{\text{envelope}} \underbrace{\left(\frac{\sin N\frac{\pi\Delta}{L\lambda}x}{\sin\frac{\pi\Delta}{L\lambda}x}\right)^2}_{\text{fine details}} \tag{3-1}$$

This is a sinc function envelope with fine details within. And as N goes to infinity, the pattern becomes an impulse train of spacing $L\lambda/\Delta$ enveloped by a sinc function. The proof is as follow:

Let the aperture function be

$$A(x) = \text{rect}\left(\frac{x}{a}\right) * \sum_{n=-\infty}^{\infty} \delta(x - \Delta)$$

Where $\text{rect}(x)$ is the rectangular function, and $*$ is the convolution operator. Then taking its Fourier transform:

$$\mathcal{F}\{A(x)\}(v) = \mathcal{F}\left\{\text{rect}\left(\frac{x}{a}\right)\right\} \times \mathcal{F}\left\{\sum_{n=0}^{N-1}\delta(x - n\Delta)\right\}$$

$$\propto \text{sinc}(av) \times \sum_{n=0}^{N-1}\left(e^{-i2\pi v}\right)^n = \left(\frac{\sin(\pi av)}{\pi av}\right)\left(\frac{1 - e^{-i2\pi v\Delta N}}{1 - e^{-i2\pi v}}\right)$$

$$= \left(\frac{\sin(\pi av)}{\pi av}\right) \cdot e^{-i\pi v\Delta(N-1)}\left(\frac{e^{i\pi v\Delta N} - e^{-i\pi v\Delta}}{e^{i\pi v\Delta} - e^{-i\pi v\Delta}}\right)$$

$$= e^{-i\pi v\Delta(N-1)}\left(\frac{\sin(\pi av)}{\pi av}\right)\left(\frac{\sin(N\pi\Delta v)}{\sin(\pi\Delta v)}\right)$$

Finally, by taking the magnitude squared and replace v with $x/L\lambda$, we obtained equation 3-1.

3.1.2. Experimental Results of Single Helix

For our experiment, we used a spring with spacing $\Delta \approx 2$ mm (the sparse part in figure 3.3), made from metal wire of thickness $a \approx 0.5$ mm. And the inclination of the wire is around $2\theta \approx 25°$.

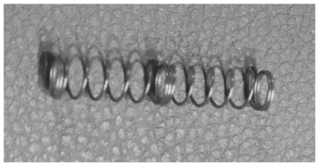

Figure 3.3 (spring)

We placed the spring $100\ \text{cm}$ away from a screen and shone a red laser of wavelength $\lambda \approx 650\ \text{nm}$ on it. The results are shown below:

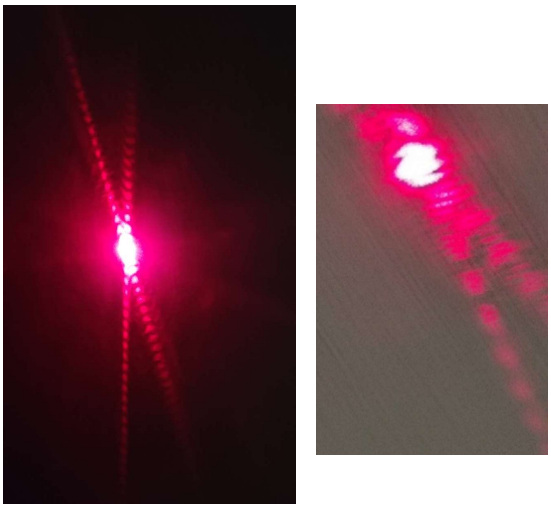

Figure 3.4 (left: X-cross, right: fine details)

Amazing! This is exactly what we have expected. The figure on the left features an evident cross, we small spots spanning across the two arms of the cross. And as we zoom in on one of the spots, we get the right figure, which contains approximately 7 fine stripe details within a single spot.

Some data measured form the picture are listed below:

Parameter	Theoretical Value	Measurement	Error
Tilt angle	$12.5°$	$10°$	0.2
Spot spacing $(L\lambda/a)$	$1.3\ \text{mm}$	$1.3\ \text{mm}$	0
Detail spacing $(L\lambda/2\Delta)$	$0.1625\ \text{mm}$	$0.186\ \text{mm}$	0.14

Table 3.1 (single helix diffraction)

The theoretical values are obtained and derived from the data of the spring. Though many of the values are mere approximates, with error far greater than just the statistical error listed in table 3.1 (type A uncertainties omitted), the order of magnitude of the results obtained from these crude data are incredibly accurate.

3.1.3. X-Ray Diffraction Pattern of DNA

Now, let us turn to the real diffraction pattern of a double helix.

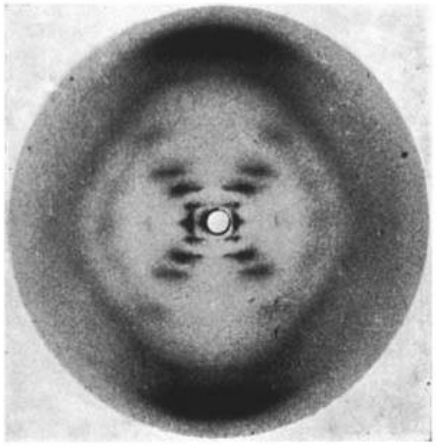

Figure 3.5 (photo 51)

"Photo 51 (figure 3.5) is an X-ray based fiber diffraction image of a paracrystalline gel composed of DNA fiber taken by Raymond Gosling, a graduate student working under the supervision of Rosalind Franklin in May 1952 at King's College London, while working in Sir John Randall's group. The image was tagged "photo 51" because it was the 51st diffraction photograph that Franklin and Gosling had taken. It was critical evidence in identifying the structure of DNA."[7]

Let us now analyze it: Since a double helix is just the superposition of two single helices that are shifted in space, we know from Fourier optics, this introduces a phase shift between the image of the two helix.

$$\mathcal{F}\{A(x+\delta)\}(\nu) = e^{i2\pi\nu\delta} \cdot \mathcal{F}\{A(x)\}(\nu) \tag{3-2}$$

More precisely, let $E(x', y')$ be the electric field of a single helix on the image plane. Now, let ζ be the spacing between the two single helices, one of the helices moves upward a distance of $\zeta/2$ while another moves downward a distance of $-\zeta/2$. Then the electric field becomes:

$$E_{\text{new}}(x', y') = E(x', y')e^{i2\pi\nu_y\frac{\zeta}{2}} + E(x', y')e^{i2\pi\nu_y\frac{-\zeta}{2}}$$

$$\nu_y = \frac{y'}{L\lambda} \rightarrow E_{\text{new}}(x', y') = 2E(x', y')\cos\left(\frac{\pi\zeta}{L\lambda}y'\right) \tag{3-2}$$

So, besides the initial diffraction pattern of a single helix, there is a new cosine-shaped envelope over the whole pattern.

We now know that the DNA in photo 51 is a B-DNA (figure 3.6), having an inclination angle of $39.7°$, a major groove of 6 b.p. (3.32 Å ascend per bonding pair), a minor groove of 4 b.p., and a diameter of 2 nm.

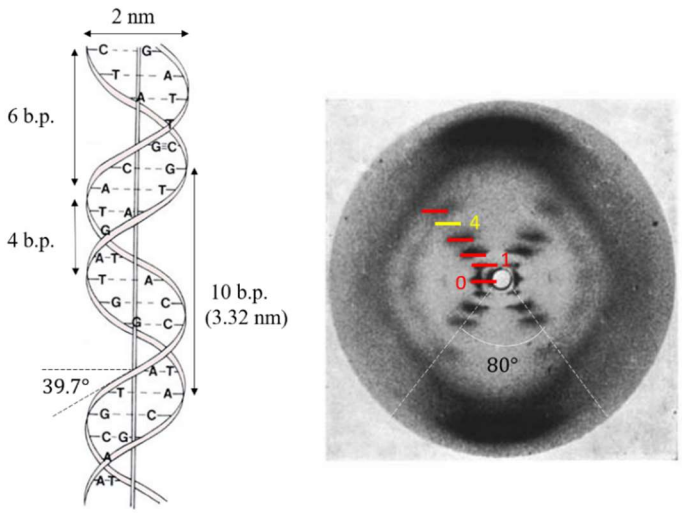

Figure 3.6 (B-DNA)

First of all, the angle between the crosses in the right of Figure 3.6 is $80° \approx 2 \times 39.7°$, as according to theoretical expectation.

Secondly, the double helix of B-DNA has three spatial periodicities, the width of a single bonding pair $a = 1$ b.p., the major/minor grooves $\zeta = 6$ b.p. (it doesn't matter if we choose ζ as 4 or 6 b.p.), and the pitch of a single turn $\Delta = 10$ b.p. From our ideas in Fourier optics and Fourier transform of impulse train, we can guess its diffraction pattern as

$$\text{Intensity} \propto \left[\frac{\sin\left(\frac{\pi a}{L\lambda}x\right)}{\frac{\pi a}{L\lambda}x}\right]^2 \left[\cos\left(\frac{\pi\zeta}{L\lambda}x\right)\right]^2 \left[\sum_{n=-\infty}^{\infty} \delta\left(\frac{x}{L\lambda} - \frac{n}{\Delta}\right)\right]^2 \tag{3-3}$$

Setting $L\lambda = 10$, $a = 1$, $\zeta = 6$, and $\Delta = 10$, we have the following plot:

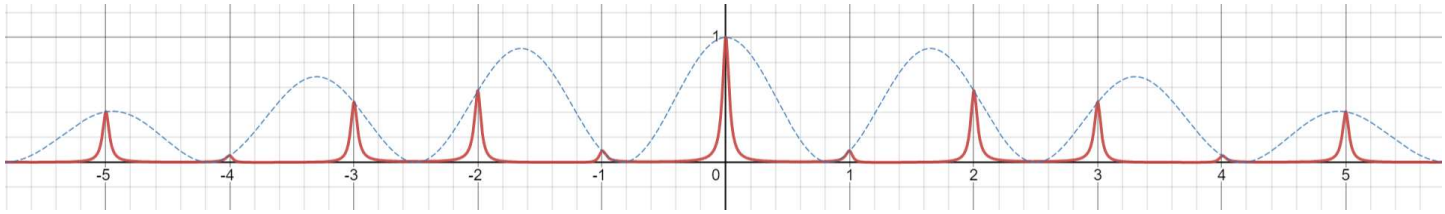

Figure 3.7 (plot of DNA diffraction)

In figure 3.7, the dashed line is the envelope cause by a and ζ, but since $\zeta > a$, the effect of the cosine envelope is more evident, and the solid line approximates the impulse train induced by Δ.

As we can clearly see, the fourth peak/bright spot is nearly gone because of the cosine envelope, as expected from the true results of photo 51.

From a single photo of DNA X-ray diffraction, so many information can be. Indeed, the power of Fourier optics is a pathway to many abilities some consider unnatural and omnipotent.

3.2. Zone Plates

3.2.1. Fresnel Half Period Zones

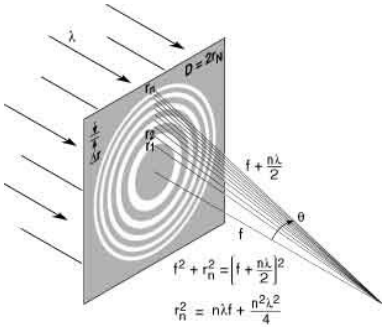

Figure 3.8 (Fresnel half period zones)

To show the properties of zone plates, we need to introduce a special aperture called “Fresnel half period zones” first.

In Fresnel half period zones, the radius of the n-th circle is defined as

$$r_n = \sqrt{n\lambda f + \frac{n^2\lambda^2}{4}} \tag{3-4}$$

Where f is the focal length of the zones and λ is the wavelength of the incidence light.

If $f \gg \lambda$, r_n can be approximated as

$$r_n \approx \sqrt{n\lambda f} \tag{3-5}$$

Now consider the OPD between two rays, a ray from the $n+1$-th circle to the focal point and a ray from the n-th circle to the focal point. The OPD will be

$$OPD = \sqrt{r_{n+1}^2 + f^2} - \sqrt{r_n^2 + f^2} = \frac{\lambda}{2} \tag{3-6}$$

That’s why the zones are called “half period.”

3.2.2. Property as Lens Derived from Fourier Optics

The aperture function of a zone plate can be express as

$$A(r) = \sum_{n=1}^{2N} (-1)^n \mathrm{cyl}\left(\frac{r}{2r_n}\right) \tag{3-7}$$

Where $\mathrm{cyl}(r/D)$ is the cylinder function.

If we place an observation plane at the focal plane of the zone plate, from the Fraunhofer approximation, the distribution of light intensity on the plane is

$$I(\rho) \propto [\mathcal{F}\{A(r)\}(\rho)]^2 = \left[\sum_{n=1}^{2N} (-1)^n r_n^2 \pi\, \mathrm{somb}(2r_n\rho)\right]^2 \tag{3-8}$$

Where $\mathrm{somb}(\rho)$ is the sombrero function, and $\rho = \sqrt{\left(\frac{x}{f\lambda}\right)^2 + \left(\frac{y}{f\lambda}\right)^2}$.

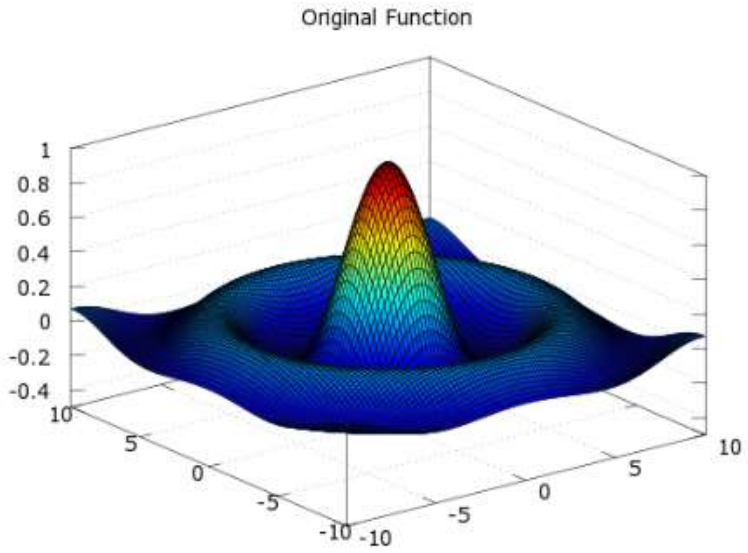

Figure 3.9 (sombrero function)

In figure 3.9, we can see that the sombrero function has its maximum value at the center and the value is much larger than other local maxima. Thus, we can safely conclude that the zone plate has the ability to focus a beam of parallel light with wavelength λ to a focal point.

3.3. Reciprocal Lattice

3.3.1. Lattices

A crystal can be described as the convolution between its lattice and its unit cell. And a general lattice in three-dimensional space can be described using the *lattice translational vectors*.

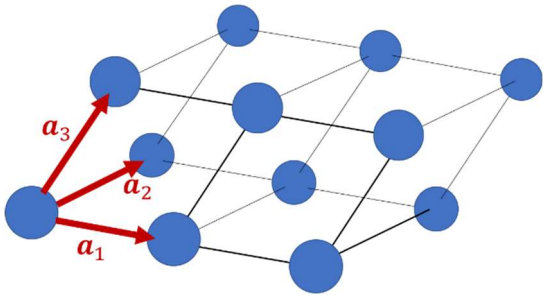

Figure 3.10 (3D lattice with lattice vectors)

Denoted as $\boldsymbol{a}_1$, $\boldsymbol{a}_2$ and $\boldsymbol{a}_3$, they are the basis vector for all lattice points, i.e. the coordinate of any lattice point can be specified as a linear combination of these three vectors:

$$\text{lattice point: } \boldsymbol{T} = n_1\boldsymbol{a}_1 + n_2\boldsymbol{a}_2 + n_3\boldsymbol{a}_3 \quad (n_1, n_2, n_3 \in \mathbb{Z}) \tag{3-9}$$

Moreover, the norm of these three vectors are also known as the *lattice constants*.

3.3.2. Reciprocal Lattice in 2D

Reciprocal lattices are the Fourier transform of real lattices! Such idea is the key to why such mathematical object is created. The mathematics of Fourier transform is essentially "encoded" into the structure of reciprocal lattice, and using the reciprocal lattice, we can gain insights into the momentum space of the lattice and even reduce calculations when figuring out the diffraction patterns of lattices under any orientation.

Without further ado, let us consider a 2D lattice and its reciprocal lattice.

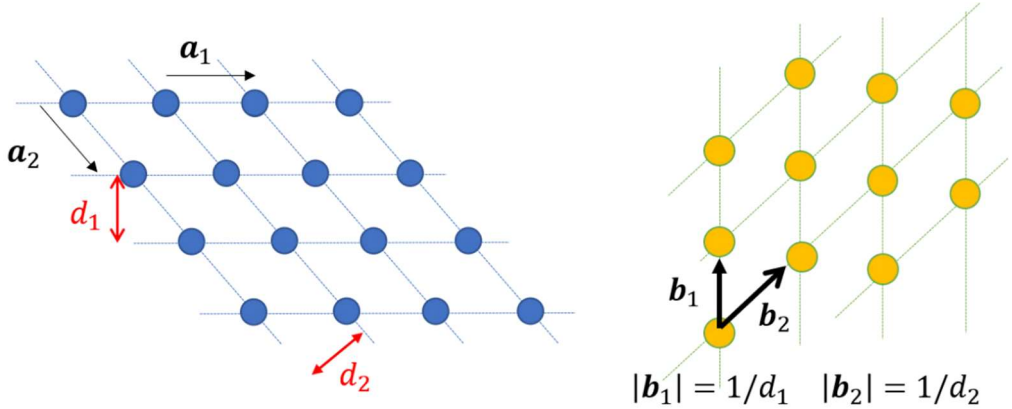

(a) 2D lattice (b) 2D reciprocal lattice

Figure 3.11 (a 2D lattice and its reciprocal lattice)

The lattice in figure 3.11-(a) is spanned by the translational vectors $\boldsymbol{a}_1$ and $\boldsymbol{a}_2$. Moreover, we can see two different families of parallel lines going through all the lattice points, having the periodic spacing of d_1 and d_2 respectively.

Now, from Fourier optics, we can figure out the diffraction pattern of the above lattice. (A) Since a lattice is just a combination of impulse trains, its Fourier transform is also an impulse train, or in layman's terms, *the Fourier transform of a lattice is just another lattice*. (B) The periodicity of the new lattice is *perpendicular* to that of the periodic parallel lines in the actual lattice. (C) The period of the Fourier transform is *inversely proportional* to the original period of the lattice. By combining the three points mentioned above, we obtained the figure 3.11-(b).

This is known as the reciprocal lattice. It is spanned by the reciprocal lattice translational vectors $\boldsymbol{b}_1$ and $\boldsymbol{b}_2$, each having the norm of $1/d_1$ and $1/d_2$ respectively, and hence the name "reciprocal" lattice. What are the relationships between all the translational vectors? From the area of the parallelogram spanned by $\boldsymbol{a}_1$ and $\boldsymbol{a}_2$, we can tell that

$$|\boldsymbol{b}_i| = \frac{|\boldsymbol{a}_i|}{|\boldsymbol{a}_1 \times \boldsymbol{a}_2|} \qquad (i = 1,2) \tag{3-10}$$

And that the vectors are orthogonal to each other, i.e.

$$\boldsymbol{a}_i \cdot \boldsymbol{b}_i = 0 \qquad (i = 1,2) \tag{3-11}$$

What's more, we can view each reciprocal lattice point as *a family of parallel lines* in the real lattice. For a given reciprocal lattice point denoted as $\boldsymbol{G} = n_1\boldsymbol{b}_1 + n_2\boldsymbol{b}_2$, this family of parallel lines will have a periodic spacing of $1/|\boldsymbol{G}|$. A single family of parallel lines should go through all lattice points.

3.3.3. Reciprocal Lattice in 3D

For a 3D lattice, with lattice translational vectors $\boldsymbol{a}_1$, $\boldsymbol{a}_2$ and $\boldsymbol{a}_3$, instead of having a parallelogram in the denominator, we should have the volume of a *parallelepiped*. Thus, its reciprocal lattice translational vectors are:

$$\boldsymbol{b}_i = \frac{\boldsymbol{a}_j \times \boldsymbol{a}_k}{|\boldsymbol{a}_1 \cdot \boldsymbol{a}_2 \times \boldsymbol{a}_3|} \tag{3-12}$$

With (i, j, k) being the cyclic permutation of $(1,2,3)$. Moreover, we can see that the orthogonal condition of equation (3-11) still holds. And each lattice point $\boldsymbol{G} = n_1\boldsymbol{b}_1 + n_2\boldsymbol{b}_2 + n_3\boldsymbol{b}_3$ represents *a family of parallel planes* that goes through all lattice points, having periodic spacing of $1/|\boldsymbol{G}|$.

3.3.4. Bragg Condition

Now let us consider what happens when a ray of light is incident on the real lattice. For the 3D case, we have:

$$\boldsymbol{a}_i \cdot \boldsymbol{b}_j = \delta_{ij} = \begin{cases} 1, & i = j \\ 0, & i \neq j \end{cases} \qquad (i, j \in \{1,2,3\}) \tag{3-13}$$

Thus, the reciprocal lattice vectors $\boldsymbol{G} = n_1\boldsymbol{b}_1 + n_2\boldsymbol{b}_2 + n_3\boldsymbol{b}_3$ can be thought of as the *frequency basis* for our Fourier series expansion, i.e.

$$n(\boldsymbol{r}) = \sum_{\boldsymbol{G}} n_{\boldsymbol{G}} e^{i2\pi \boldsymbol{G}\cdot\boldsymbol{r}} \tag{3-14}$$

Where $\boldsymbol{r}$ is the position vector of real space, $n_{\boldsymbol{G}}$ are the Fourier coefficients, and the index $\boldsymbol{G}$ runs through all possible reciprocal lattice vectors/points. We can check that such decomposition is valid simply by checking whether it preserves the periodicity of the lattice. Let $\boldsymbol{T} = n_1\boldsymbol{a}_1 + n_2\boldsymbol{a}_2 + n_3\boldsymbol{a}_3$ be a lattice translational vector, then

$$n(\boldsymbol{r}+\boldsymbol{T}) = \sum_{\boldsymbol{G}} n_{\boldsymbol{G}} e^{i2\pi \boldsymbol{G}\cdot(\boldsymbol{r}+\boldsymbol{T})} = \sum_{\boldsymbol{G}} n_{\boldsymbol{G}} e^{i2\pi \boldsymbol{G}\cdot\boldsymbol{r}} e^{i\boldsymbol{G}\cdot\boldsymbol{T}} = \sum_{\boldsymbol{G}} n_{G} e^{i2\pi \boldsymbol{G}\cdot\boldsymbol{r}} = n(\boldsymbol{r}) \tag{3-15}$$

Now back to the diffraction off a lattice: the incident ray will deflect off the lattice in a new direction, with a change in the wavevector $\Delta\boldsymbol{k} \coloneqq \boldsymbol{k}' - \boldsymbol{k}$, as shown in the figure 3.12 below.

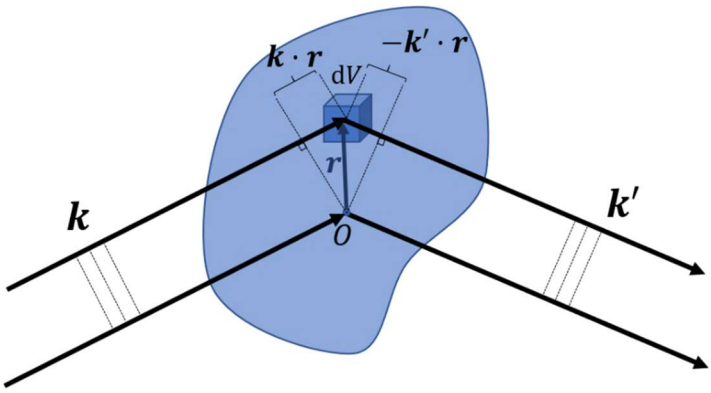

Figure 3.12 (ray diffracted from a lattice)

The strength of a ray diffracted from an infinitesimal volume $\mathrm{d}V$ located at $\boldsymbol{r}$ is proportional to the electron density $n(\boldsymbol{r})$ there. Moreover, consider the phase difference between the ray and another that diffracted from the origin:

$$\Delta\phi = (\boldsymbol{k}\cdot\boldsymbol{r}) + (-\boldsymbol{k}'\cdot\boldsymbol{r}) = -(\boldsymbol{k}'-\boldsymbol{k})\cdot\boldsymbol{r} \coloneqq -\Delta\boldsymbol{k}\cdot\boldsymbol{r} \tag{3-16}$$

Thus, the total strength of diffracted ray will be proportional to

$$\int_{\mathbb{R}^3} n(\boldsymbol{r}) e^{-i\Delta\boldsymbol{k}\cdot\boldsymbol{r}}\,\mathrm{d}V = \sum_{G}\int_{\mathbb{R}} n_{\boldsymbol{G}} e^{i2\pi\boldsymbol{G}\cdot\boldsymbol{r}} e^{-i\Delta\boldsymbol{k}\cdot\boldsymbol{r}}\,\mathrm{d}V = \sum_{G}\int_{\mathbb{R}} n_{\boldsymbol{G}} e^{i(2\pi\boldsymbol{G}-\Delta\boldsymbol{k})\cdot\boldsymbol{r}}\,\mathrm{d}V \tag{3-17}$$

The integral above reaches its maxima if $2\pi\boldsymbol{G} - \Delta\boldsymbol{k} = 0$. Therefore, bright spots of diffraction will appear if it satisfies this "Bragg condition":

$$\boxed{\Delta\boldsymbol{k} = 2\pi\boldsymbol{G}} \tag{3-18}$$

Is the Bragg condition mentioned above connected to the Bragg law we've learnt from senior high? Yes, they are connected! And in fact, they are identical to each other.

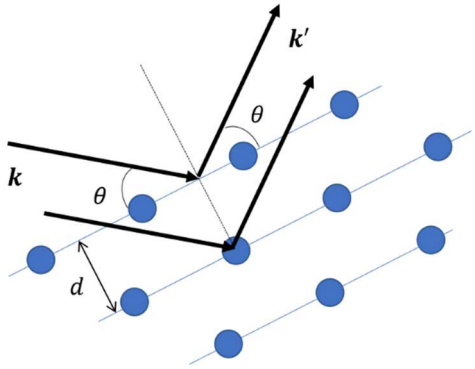

Figure 3.13 (Bragg diffraction on real lattice)

The Bragg law states that constructive interference occurs when

$$2d\sin\theta = m\lambda \qquad (m \in \mathbb{N}) \tag{3-19}$$

But since the periodic spacing $d = m/|\boldsymbol{G}|$, let $\hat{\boldsymbol{n}}$ be the direction of $\boldsymbol{G}$ (or the direction of d), we have, for the change in wavevector:

$$\Delta\boldsymbol{k} = 2k\sin\theta\,\hat{\boldsymbol{n}} = 2\frac{2\pi}{\lambda}\sin\theta\,\hat{\boldsymbol{n}} = 2\pi\frac{m}{d}\hat{\boldsymbol{n}} = 2\pi\boldsymbol{G}$$

This is exactly the Bragg condition we obtained as equation (3-18).

3.3.5. Diffraction Pattern of Lattice

We've finally reached the capstone, let us now discuss how we can use the reciprocal lattice in problems regarding lattice X-ray crystallography (diffraction pattern). And besides the Bragg condition mentioned above, the wavevector must also satisfy the fact that its norm doesn't change before and after diffraction. Thus, we have the following two diffraction conditions for constructive interference patterns:

$$\begin{aligned}\Delta\boldsymbol{k} &= 2\pi\boldsymbol{G}\\ |\boldsymbol{k}| &= |\boldsymbol{k}'|\end{aligned} \tag{3-20}$$

If we let the incident $\boldsymbol{k}$ be perpendicular to the imaging plane that is at a distance L away, then $\Delta\boldsymbol{k}$ represents the sideways component of the diffracted rays, as shown in figure 3.14. Bright interference spots appear at

$$x' = L\tan\theta = L\tan\left[\arccos\left(1 - \frac{|\Delta\boldsymbol{k}|^2}{2|\boldsymbol{k}|^2}\right)\right] \tag{3-21}$$

For a known input ray, all we have to do now is to find all the possible $\Delta\boldsymbol{k}$ vectors, then we can identify the diffraction patterns! For this, let us look back into the reciprocal lattices.

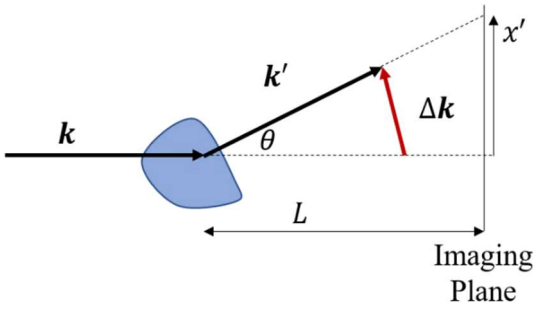

Figure 3.14 (diffraction through a lattice)

The second condition, $|\boldsymbol{k}| = |\boldsymbol{k}'|$, places restriction on the magnitude of $\Delta\boldsymbol{k}$ (or $\boldsymbol{G}$). It isn't hard to see that it is a sphere (circle if in 2D) in the reciprocal lattice space with a diameter of $2/\lambda$, known as the *Ewald's sphere*. Moreover, we know that constructive interference is found only when a $\boldsymbol{G} = n_1\boldsymbol{b}_1 + n_2\boldsymbol{b}_2 + n_3\boldsymbol{b}_3$ is found on the sphere drawn. Take a 2D case for example:

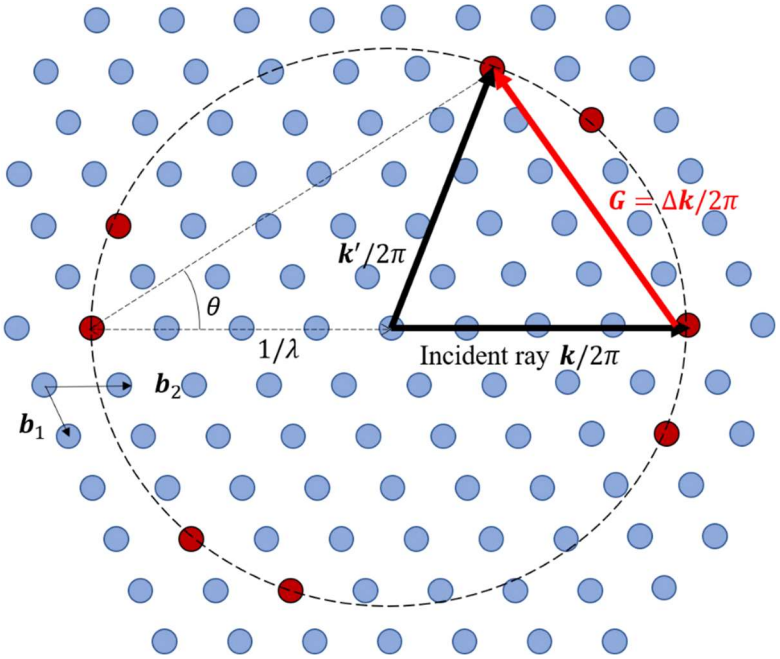

Figure 3.15 (diffraction in reciprocal lattice)

Placing the *tip of the incident ray* on one of the reciprocal lattice points, we can figure out the possible diffracted ray. And amazingly, diffraction in the reciprocal lattice is equivalent to finding points intersected by a circle with radius $1/\lambda$. The angle θ is the Bragg diffraction angle. We can see that there are more than one possible diffraction directions. Thus, for the orientation of this lattice with respect to the incident ray, there will be 8 constructive interference spikes detected (in figure 3.16). And from the geometry of figure 3.15, we can also see that the diffraction angle (the direction of the diffracted ray) is twice that of the Bragg angle θ_B.

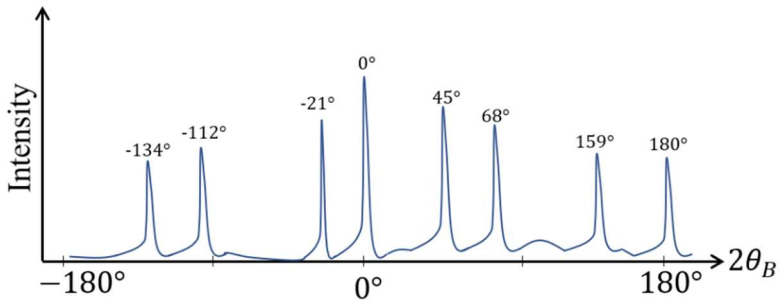

Figure 3.16 (estimated intensity of lattice diffraction)

Moreover, if we were to consider the diffraction pattern of a "powder", the tools we generalized from reciprocal lattice can even outperform that of Fourier optics. In a powder, crystals orient in different directions, thus, the reciprocal lattice space have different orientations with respect to the incident wave.

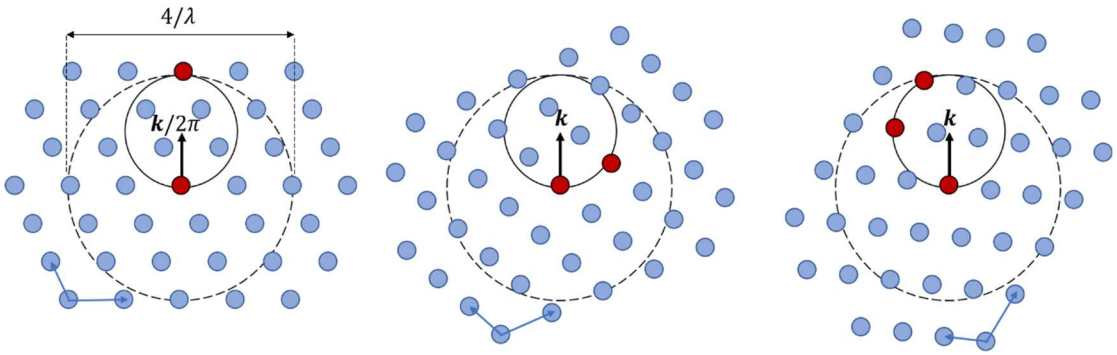

Figure 3.17 (reciprocal lattice of many orientations)

As can see from above, as we go through all possible orientation of the lattice, all the reciprocal lattice points within the circle of diameter of $4/\lambda$ will be intersected by the small circle generated from $|\boldsymbol{k}| = |\boldsymbol{k}'|$, i.e. they will be part of the diffraction pattern. Thus, we shall obtain the concentric circle diffraction patterns of figure 3.18, known as the *Debye-Scherrer rings*.

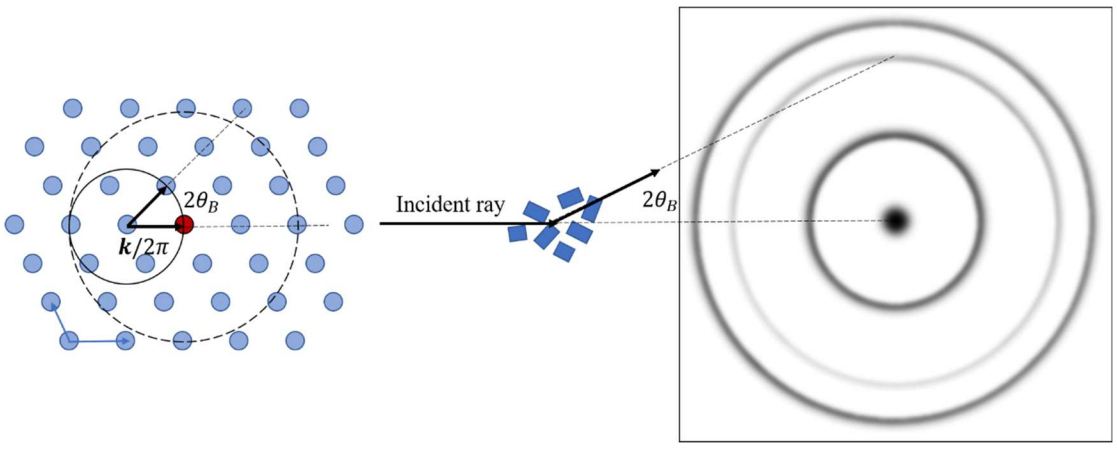

Figure 3.18 (powder diffraction)

4. References

[1] Optics, 5th edition; Ajoy Ghatak, McGraw-Hill Education; Ch.19, Ch.20

[2] Intro to diffraction; Patrick Shamberger, YouTube; 2022/5/20

[3] Fourier Optics; Jordan Edmunds, YouTube; 2022/5/20

[4] Figure 1.2: Fundamentals of Photonics; Bahaa E. A. Saleh, Malvin Carl Teich; 1991 John Wiley & Sons, Inc.

[5] Figure 3.8: https://xdb.lbl.gov/Section4/Image_Sec4/Sec4421.jpg

[6] Figure 3.5: https://www-project.slac.stanford.edu/wis/images/photo_51.jpg

[7] Photo 51, Wikipedia: https://en.wikipedia.org/wiki/Photo_51; 2022/6/2

[8] Figure 3.6: https://pansci.asia/archives/59684

[9] Diffraction Pattern of DNA; https://physicsopenlab.org/2019/10/01/double-helix-optical-diffraction-pattern/; 2022/6/2